Biogeosciences Discuss., https://doi.org/10.5194/bg-2019-132
Manuscript under review for journal Biogeosciences
Discussion started: 23 April 2019

Major role of ammonia-oxidizing bacteria in N_2O production in the Pearl River Estuary

Li Ma[1,2], Hua Lin[1,2,3], Xiabing Xie[1], Minhan Dai[1,2], Yao Zhang[1,2]

[1]State Key Laboratory of Marine Environmental Science, Xiamen University, Xiamen 361101, China

[2]College of Ocean and Earth Sciences, Xiamen University, Xiamen 361101, China

[3]Key Laboratory of Marine Ecosystem and Biogeochemistry, State Oceanic Administration, Second Institute of Oceanography, Ministry of Natural Resources, Hangzhou 310012, China

Correspondence to: Yao Zhang (yaozhang@xmu.edu.cn)

Abstract. Nitrous oxide (N_2O) has significant global warming potential as a greenhouse gas. Estuarine and coastal regimes are the major zones of N_2O production in the marine system. However, biological sources of N_2O in estuarine ecosystems remains controversial, but is of great importance for understanding the global N_2O emission patterns. Here, we measured concentrations and isotopic compositions of N_2O as well as distributions and transcript levels of ammonia-oxidizing bacterial and archaeal *amo*A and denitrifier *nir*S genes by quantitative polymerase chain reaction along a salinity gradient in the Pearl River Estuary, and performed in situ incubation experiments to estimate N_2O yields. Our results indicated that nitrification predominantly occurred, with significant N_2O production during ammonia oxidation, in the hypoxic waters of the upper estuary where the maximum N_2O and ΔN_2O concentrations were observed, although minor denitrification might be concurrent at the site with the lowest dissolved oxygen. Ammonia-oxidizing β-proteobacteria (AOB) were significantly positively correlated with all N_2O parameters, although their *amo*A gene abundances were distinctly lower than ammonia-oxidizing Archaea (AOA) throughout the estuary. Furthermore, the N_2O production rate and the N_2O yield normalized to *amo*A gene copies or transcripts estimated a higher relative contribution of AOB to the N_2O production in the upper estuary. Taken together, the in situ incubation experiments, N_2O isotopic composition and concentrations, and gene datasets suggested that the high concentration of N_2O (oversaturated) is mainly produced from strong nitrification by the relatively high abundance of AOB in the upper reaches as the major source of N_2O emitted to the atmosphere in the whole estuary.

Biogeosciences Discuss., https://doi.org/10.5194/bg-2019-132
Manuscript under review for journal Biogeosciences
Discussion started: 23 April 2019

1 Introduction

Nitrous oxide (N_2O) is a potent greenhouse gas with global warming potential 298 times that of carbon dioxide (CO_2) on a 100 yr timescale, and contributes to stratospheric ozone depletion as a major precursor of free radicals (Ravishankara et al., 2009). N_2O emissions from soils and marine systems are estimated to account for 56%–70% (6–7 Tg N_2O-N yr^{-1}) (Syakila and Kroeze, 2011; Butterbach-Bahl et al., 2013; Hink et al., 2017) and 30% (4 Tg N_2O-N yr^{-1}) (Nevison et al., 2004; Naqvi et al., 2010; Voss et al., 2013) of the total global N_2O emissions, respectively. The main processes responsible for N_2O emissions are microbial transformation of ammonia, nitrite, and nitrate through nitrification and denitrification (Butterbach-Bahl et al., 2013). It has been estimated that oceanic N_2O production is dominated by nitrification, whereas only 7% is contributed by denitrification (Freing et al., 2012).

N_2O is released as a byproduct during nitrification via incomplete oxidation of hydroxylamine (NH_2OH) to nitrite (NO_2^-) by ammonia-oxidizing bacteria (AOB) (Stein, 2011). This process may be enhanced under suboxic conditions (Naqvi et al., 2010). While no equivalent of the hydroxylamine-oxidoreductase that catalyzes N_2O formation through NH_2OH oxidation has been found in ammonia-oxidizing archaea (AOA) (Hatzenpichler, 2012), recent studies indicated that AOA possibly produces hybrid N_2O via a combination of an ammonia oxidation intermediate (NH_2OH, HNO, or NO) and NO_2^- (Stiglmeier et al., 2014; Frame et al., 2017). In addition, AOB have been shown to produce N_2O from NO_2^- during nitrifier denitrification (Shaw et al., 2006). This process is also promoted under micro-oxic and anoxic conditions (Yu et al., 2010). Denitrification by heterotrophic denitrifiers is another major pathway of N_2O production in marine environments. NO_2^- is reduced by a copper-containing (NirK) or cytochrome cd1-containing nitrite reductase (NirS) to nitric oxide (NO), and then by a heme-copper NO reductase (NOR) to N_2O.

Biological nitrogen transformations are catalyzed by various microbial enzymes, of which ammonium monooxygenase (AMO) and nitrite reductases (NIRs) are key enzymes responsible for nitrification and denitrification, respectively (Canfield et al., 2010). The genes encoding for AMO subunit A (*amo*A) and NIRs (*nir*S and *nir*K) have been widely applied as functional marker genes to identify the distribution of ammonia oxidizers and denitrifiers. Previous studies have shown significant correlations of *amo*A with spatial variations of N_2O emissions or N_2O production rates in soils and

oceans (Avrahami and Bohanann, 2009; Santoro et al., 2011; Löscher et al., 2012). In addition, significant relationships between *nir*K or *nir*S abundance and N_2O emissions were observed in grassland (Čuhel et al., 2010) and arable (Clark et al., 2012; Jones et al., 2014) soils, and the ocean (Arévalo-Martínez et al., 2015).

Estuarine and coastal regimes have long been recognized major zones of N_2O production in the marine system (Seitzinger and Kroeze, 1998; Mortazavi et al., 2000; Usui et al., 2001; Kroeze et al., 2010; Allen et al., 2011). Although AOA frequently outnumber AOB and dominate in abundance, their contribution to nitrification remains controversial in estuarine and coastal waters (Bernhard et al., 2010; Zhang et al., 2014; Hou et al., 2018); additionally, the relative contributions of AOB and AOA to N_2O production is inconclusive (Monteiro et al., 2014). Moreover, there is a potential niche overlap between nitrifiers and denitrifiers in low oxygen conditions. AOB are reported to thrive in hypoxic environments, and denitrification in the oxic ocean is suggested to occur within anaerobic particle interiors (Frame and Casciotti, 2010; Ni et al., 2014). It is therefore of great importance to elucidate the biological sources of N_2O production in estuarine ecosystems to better understanding the global N_2O emission patterns.

The Pearl River Estuary (PRE) is one of the world's most complex estuarine systems with runoff ranked 17th of the world rivers (Dai et al., 2014). The PRE is surrounded by complex regions that supply rich nitrogen inputs and produce eutrophic waters that support active nitrification (Dai et al., 2008). Moreover, increased oxygen consumption by organic matter degradation leads to the formation of hypoxic zones in the upper reaches of the PRE (Dai et al., 2006; He et al., 2014), which support (de)nitrification and N_2O production (Lin et al., 2016).

In this study, N_2O-related biogeochemical parameters were measured, and distributions and transcript levels of AOB and AOA *amo*A and denitrifier *nir*S genes were quantified by quantitative polymerase chain reaction (qPCR) to investigate the relationship between N_2O production and spatial distribution of AOA and AOB along a salinity gradient in the PRE (Fig. 1). Moreover, in situ incubation experiments were performed in the hypoxic upper estuary to estimate (1) nitrification rates and N_2O production rates, (2) whether denitrification occurred during nitrification, and (3) N_2O yield (μmol N_2O produced per mol ammonia oxidized). By combining the genetic datasets and incubation estimates, this study thus identified the relative contributions of AOB and AOA in producing N_2O in the PRE.

Biogeosciences Discuss., https://doi.org/10.5194/bg-2019-132
Manuscript under review for journal Biogeosciences
Discussion started: 23 April 2019

2 Materials and methods

2.1 Study area and sampling

A total of 22 sites along the salinity gradient of the PRE were sampled during a cruise in July 2015, including 11 sites in the upper reaches (upstream of the Humen outlet) and 11 sites in the lower reaches (Lingdingyang) (Fig. 1). Water samples were taken from the surface (2 m) and bottom (4–15 m) of each site by using a conductivity, temperature, and depth (CTD) rosette sampling system (SBE 25; SeaBird Inc, USA) fitted with 12 L Niskin bottles (General Oceanics). A total of 16 samples (from two depths at eight sites) were subjected to gene analysis (Fig. 1). One liter of water for gene analysis was filtered through 0.8 μm and then 0.22 μm pore size polycarbonate membrane filters (47 mm diameter, Millipore) within 30 min at a pressure <0.03 MPa to retain the particle-associated (PA) communities (>0.8 μm) and free-living (FL) communities (0.22–0.8 μm). RNAlater solution (Ambion, Austin, Texas, USA) was quickly added into the samples to prevent RNA degradation. All of the filters were immediately flash frozen in liquid nitrogen and then stored at -80 ℃ until further analysis. Water samples for nutrient determination were filtered through 0.45 μm pore size cellulose acetate membranes and then immediately frozen at -20 ℃ until further analysis. Ammonia/ammonium concentrations were analyzed onboard. Water samples for dissolved N_2O were collected into 125 mL headspace glass bottles to which 100 μL of saturated $HgCl_2$ was added; the bottles were immediately closed with rubber stoppers and aluminum crimp-caps and were stored in the dark at 4 ℃ until analysis in the laboratory. All N_2O samples were collected during the July 2015 cruise except for part samples (from sites P03, P05, A01, A06, and A10) intended for N_2O isotopic composition analyses, which were sampled during a cruise in March 2010. Total suspended material (TSM) was collected by filtering 1–4 L of water onto pre-combusted and pre-weighed glass fiber filter (GF/F) membranes (Whatman), and then stored at -20 ℃ until weighing in the laboratory.

2.2 Biogeochemical parameters, N_2O emissions, and isotopic analysis

Temperature and salinity were continuously measured with the CTD system. Dissolved oxygen (DO) concentrations were measured with a DO probe and calibrated on board by the Winkler method (Dai et al., 2006). Ammonia was measured using the indophenol blue spectrophotometric method (Pai et al.,

2001); nitrate, nitrite, and silicate were analyzed with the routine spectrophotometric methods with a Technicon AA3 Auto-Analyzer (Bran-Lube, GmbH) (Han et al., 2012). N_2O concentrations were analyzed by gas chromatography (Agilent 6890 μECD) coupled to a purge-trap system (Tekmar Velocity XPT) at 25 ℃ (Lin et al., 2016).

The excess N_2O (ΔN_2O) and N_2O saturation were calculated with Eq. (1) and (2):

$$\Delta N_2O = N_2O_{aquatic} - N_2O_{equilibrium} \quad (1)$$

$$S(\%) = N_2O_{aquatic} / N_2O_{equilibrium} \times 100\% \quad (2)$$

where $N_2O_{aquatic}$ represents the measured concentrations of N_2O in the water, and the equilibrium values of N_2O are calculated by Eq. (3) and (4) (Weiss and Price, 1980):

$$N_2O_{equilibrium} = xF \quad (3)$$

$$\ln F = A_1 + A_2(100/T) + A_3 \ln(T/100) + A_4(T/100)^2 + S[B_1+B_2(T/100) + B_3(T/100)^2] \quad (4)$$

where x is the mole fraction of N_2O in the atmosphere. In this study, we used the global mean atmospheric N_2O (327 ppb) from 2015 (http://www.esrl.noaa.gov/gmd).

The N_2O flux (F_{N2O}, μmol m^{-2} d^{-1}) through the air–sea interface was estimated based on Eq. (5):

$$F_{N2O} = k_{N2O} \times \rho \times K_H^{N2O} \times \Delta pN_2O = k_{N2O} \times 24 \times 10^{-2} \times (N_2O_{aquatic} - N_2O_{equilibrium}) \quad (5)$$

where k (cm h^{-1}) is calculated using Eq. (6) and (7) (Wanninkhof, 1992) and k_{600} is used for a freshwater system (Raymond and Cole, 2001):

$$k = 0.31 \times u^2_{av} \times (S_c/600)^{-0.5} \quad (6)$$

$$S_{c\ N2O} = 2055.6 - 137.11\ t + 4.3173\ t^2 - 0.05435\ t^3 \quad (7)$$

To determine the isotopic composition of N_2O, the gas samples were introduced into a trace gas cryogenic pre-concentration device (PreCon, Thermo Finnigan) as described in Cao et al. (2008) and Zhu et al. (2008), and then $\delta^{15}N_{N2O}$ was analyzed using an isotope ratio mass spectrometer (IRMS, Thermo Finngan MAT-253, Bremen, Germany).

2.3 Nucleic acid extraction and quantitative PCR

DNA was extracted using the FastDNA™ SPIN Kit for Soil (MP, USA) according to the manufacturers' protocol with minor modifications. RNA was extracted using TRIzol reagent (Ambion, Austin, Texas, USA), and then eluted with 50 μL of RNase-free water. The extracted RNA was treated with DNase I

(Invitrogen, Carlsbad, CA) to remove any residual DNA. DNA contamination was checked by amplifying the bacterial 16S rRNA genes before reverse transcription. Total RNA without DNA contamination was reverse transcribed to synthesize single-strand complementary DNA (cDNA) using the First-Strand cDNA Synthesis Kit (Invitrogen, Austin, Texas, USA).

The transcript and copy abundances of bacterial and archaeal *amo*A genes and bacterial *nir*S genes were examined using qPCR and a CFX96 Real Time PCR system (BIO-RAD, Singapore). The *β*-proteobacterial and archaeal *amo*A were amplified using primer sets amoA-1F and amoA-2R (Kim et al., 2008) and Arch-amoAF and Arch-amoAR (Francis et al., 2005), respectively; *nir*S was amplified using primers nirS-1F and nirS-3R (Braker et al., 1998; Huang et al., 2011). Quantitative PCR amplification for the *β*-proteobacterial and archaeal *amo*A were carried out as described previously (Mincer et al., 2007; Hu et al., 2011). For the amplification of *nir*S, the qPCR reaction mixture was prepared in accordance with Zhang et al. (2014) and thermal cycling conditions were applied as described by Huang et al. (2011). Standards for the qPCR reactions consisted of serial 10-fold dilutions (10^7 to 10^0 copies per uL) of plasmid DNA containing amplified fragments of the targeted genes (accession numbers MH458281 for *β*-proteobacterial *amo*A, KY387998 for archaeal *amo*A, and KF363351 for *nir*S). The amplification efficiencies of qPCR were always between 85%–95% with R^2 >0.99. The specificity of the qPCR reactions was confirmed by melting curve analysis, agarose gel electrophoresis and sequencing analysis. Inhibition tests were performed by 2-fold and 5-fold dilutions of all samples and indicated that our samples were not inhibited.

2.4 Incubation experiments

Incubation experiments were performed in the surface and bottom waters at sites P01 (2 and 5 m water depth) and P05 (2 and 12 m) upstream of the Humen outlet (Fig. 1). Water samples were collected from Niskin bottles through a clean Teflon® silicone hose, and were carefully filled into 125 mL cleaned headspace glass bottles without gas bubbles. The bottles were immediately closed with an air-tight butyl rubber stopper and aluminum crimp-cap. A total of 43 bottles were set up for either depth at sites P01 and 34 bottles for either depth at P05. Samples from four parallel bottles were taken to determine the initial (t_0) dissolved N_2O concentration, and triplicate samples were taken to measure the initial

dissolved inorganic nitrogen (DIN) concentration, which included ammonium, nitrite, and nitrate. The remaining 36 (P01) and 27 (P05) bottles were incubated in the dark at in situ temperatures (±1 ℃). At site P01, samples from six parallel bottles were taken at 3, 6, 18, and 24 h during the incubation experiment for N_2O determination after injecting saturated mercuric chloride ($HgCl_2$, volume ratio of 1:100) into the bottles; triplicate samples were also taken at the same time for DIN measurements by filtering through 0.7 μm pore size GF/Fs under pressure <0.03 MPa. Concentrations of N_2O, ammonium, nitrite, and nitrate were measured as described in Sect. 2.2. At site P05, samples were taken after 3, 6, and 12 h incubation and the other procedures were the same as described for site P01.

The effect of DIN assimilation is negligible during incubation in the dark (Ward, 2008). Therefore, the potential processes of nitrogen transformation and N_2O production can be determined according to "mass balance" in a closed incubation system. The main processes were analyzed based on the dynamic variations of DIN (ΔDIN), ammonia (ΔNH_4^+), nitrite (ΔNO_2^-), nitrate (ΔNO_3^-), and N_2O (ΔN_2O) concentrations during incubation. The average rates of nitrification and N_2O production were estimated using the slopes of the linear regression between concentrations versus incubation time when DIN was in balance (i.e. no denitrification).

During nitrification, NO_2^- is an intermediate product accumulated from ammonia oxidation that is then further oxidized to nitrate. Thus, the N_2O yield was calculated with Eq. (8) or (9):

$$N_2O_{yield}\ (‰) = \Delta N_{N2O} / \Delta N_{NH3} \quad (8)$$

$$N_2O_{yield}\ (‰) = \Delta N_{N2O} / \Delta N_{(NO2- + NO3-)} \quad (9)$$

2.5 Statistical analyses

Since normal distribution of the individual data sets was not always met, we used the non-parametric Wilcoxon rank-sum tests for comparing two variables. The bivariate correlations between environmental factors and functional genes were described by Spearman correlation coefficients (R value) and two-tailed tests (*P* value). The maximum gradient length of detrended correspondence analysis was shorter than 3.0, thus redundancy analysis (RDA) based on the qPCR data was used to analyze variations in the communities under the environmental constraints in the software R (version 3.4.4) Vegan 2.5–3 package. The qPCR-based relative abundances and environmental factors were

normalized via Z transformation (Magalhães et al., 2008). The null hypothesis, that the community was independent of environmental parameters, was tested using constrained ordination with a Monte Carlo permutation test (999 permutations). Standard and Partial Mantel tests were run in R (version 3.4.4) Vegan 2.5–3 package to determine the correlations between environmental factors and ammonia oxidizer compositions. Dissimilarity matrices of ammonia oxidizer communities and environmental factors were based on Bray-Curtis and Euclidean distances between samples, respectively. Based on Kendall's product-moment correlation, the significance of the Mantel statistics was obtained after 999 permutations. Statistical tests were assumed to be significant at a *P* value of <0.05.

3 Results

3.1 Distribution of nutrients, DO, and N_2O along a salinity transect of the PRE

The studied transect was divided into a northern region upstream of the Humen outlet and southern area (Lingdingyang) (Fig. 1); these regions have distinct biogeochemical characteristics. Salinity exhibited low values (0.1 to 4.4) upstream of the Humen outlet, and sharply increased from 0.7 to 34.2 downstream in Lingdingyang (Fig. 2a). The ammonium/ammonia concentrations decreased from 167.2 μmol L^{-1} (site P01 surface water) to 20.9 μmol L^{-1} (site P07 bottom water) upstream of the Humen outlet and consistently decreased downstream in Lingdingyang (5.7 μmol L^{-1} to below detection limit) (Fig. 2b). Correspondingly, the sum of nitrate and nitrite concentrations increased from 93.6 μmol L^{-1} (site P01 bottom water) to 172.3 μmol L^{-1} (site P03 surface water) upstream, but it sharply decreased seaward to Lingdingyang (Fig. 2c). The DO concentrations were distinctly lower upstream of the Humen outlet with nearly one-half of the samples below the hypoxic threshold (63.0 μmol L^{-1}; Rabalais et al., 2010). Generally, the DO concentrations increased seaward from 155.7 to 238.0 μmol L^{-1} in the surface waters of the Lingdingyang area, whereas they varied from 74.0 to 183.3 μmol L^{-1} in the bottom waters (Fig. 2d).

In contrast to the DO concentrations, the N_2O concentrations were distinctly higher upstream of the Humen outlet (48.9–148.2 nmol L^{-1}) than in Lingdingyang, where they decreased seaward from 24.6 to 5.4 nmol L^{-1} (Fig. 2e). Similarly, higher ΔN_2O (42.0–141.3 nmol L^{-1}) with saturations from 701.1% to

2175.1% was observed upstream; lower ΔN_2O (-1.4–17.8 nmol L^{-1}) was present in the Lingdingyang area with the saturations ranging from 86% to 363% (Fig. 2f). The estimated water–air N_2O fluxes were 100.4 to 344.0 μmol m^{-2} d^{-1} upstream and decreased in Lingdingyang (42.4 to -2.6 μmol m^{-2} d^{-1}) (Fig. 2g). Therefore, the entire PRE acts as a N_2O source that releases to the atmosphere and, notably, a significant negative relationship was observed between ΔN_2O, N_2O flux, and DO (P <0.01 for each) (Fig. 2i and j). The isotopic compositions of N_2O ($\delta^{15}N_{N2O}$) showed an enrichment of $^{15}N_2O$ seaward, varying from -27.9 to 7.1‰ (Fig. 2h). Overall, upstream of the Humen outlet was characterized by hypoxic waters rich in nitrogen-based nutrients, where ammonium concentrations decreased and the sum of nitrite and nitrate concentrations increased seaward, corresponding to distinctly higher N_2O fluxes released to the atmosphere.

3.2 Distributions and transcript levels of *amo*A and *nir*S genes along the salinity transect

The total abundance of AOA *amo*A (sum of FL and PA communities) varied from 3.10×10^3 to 6.87×10^5 copies L^{-1} in the surface waters (Fig. 3a) and 6.40×10^4 to 4.21×10^7 copies L^{-1} in the bottom waters; an increase along the salinity transect was observed in the bottom (Fig. 3b). In contrast, the total abundance of AOB *amo*A generally decreased seaward along the salinity transect for the surface (4.23×10^2 to 2.13×10^4 copies L^{-1}) and bottom waters (4.49×10^3 to 8.79×10^4 copies L^{-1}) (Fig. 3c and d). Overall, the abundance of AOA *amo*A was significantly higher than AOB (P <0.01). The total abundance of *nir*S varied from 9.12×10^4 to 2.00×10^7 copies L^{-1} and was higher than both AOA (P <0.05) and AOB *amo*A (P <0.01) in the surface waters and AOB *amo*A in the bottom water (P <0.01) (Fig. 3e and f). Notably, these three genes were predominantly distributed in the PA communities compared to the FL communities in the PRE transect (Fig. 3). The transcripts of the three genes were analyzed in the PA communities of the two incubation sites upstream of the Humen outlet. The transcript abundances of AOA *amo*A (7.44×10^3 to 4.62×10^5 transcripts L^{-1}) were one to three orders of magnitude higher than AOB *amo*A (3.62×10^2 to 5.00×10^2 transcripts L^{-1}) at P01 (Fig. 3a–d), whereas the transcript abundances of AOB *amo*A were relatively higher at P05 (AOB = 8.96×10^4 to 3.83×10^5 transcripts L^{-1}; AOA = 1.26×10^4 to 1.39×10^5 transcripts L^{-1}). The *nir*S gene showed a similar transcript level with AOA *amo*A

at P01 (2.20×10^4 to 6.69×10^4 transcripts L^{-1}) but one order of magnitude lower transcript level than both AOA and AOB *amo*A at P05 (8.59×10^3 to 1.12×10^4 transcripts L^{-1}) (Fig. 3e and f).

3.3 Nitrogen transformation and N_2O production in the incubation experiments

The in situ biogeochemical conditions of the incubation experiments are shown in Fig. 2 and listed in Table S1. Site P01 exhibited the lowest in situ DO concentrations (30.0 μmol L^{-1} in the bottom water and 30.9 μmol L^{-1} in the surface water). The concentration of DIN was generally unchanged in the early-to-middle (0–18 h) phase for the P01 surface water and early (0–6 h) phase for the P01 bottom water, but showed a distinct decrease in the ending phase (Fig. 4a). The ammonia and nitrite concentrations consistently decreased and increased, respectively, during the incubation experiments, but the nitrate concentrations decreased in the ending phase after a slight increase (Fig. 4b). These results clearly indicate that nitrification occurred during the entire P01 incubations, and suggest that denitrification may be present in the ending phase. The rates of ammonia oxidation during the entire incubations and nitrite oxidation during the early or early-to-middle phases were estimated by linear regressions of ammonia and nitrate concentrations, respectively (Fig. 4a and b; Table 1). Correspondingly, the estimated average N_2O production rate (24 h) was 0.62 nmol $L^{-1}h^{-1}$ in P01 surface water and 0.70 nmol $L^{-1}h^{-1}$ in P01 bottom water; the estimated N_2O production rates from nitrification were 0.60 nmol $L^{-1}h^{-1}$ in the surface water (18 h) and 1.61 nmol $L^{-1}h^{-1}$ in the bottom water (6 h; Fig. 4c). Thus, the estimated N_2O yield in the surface and bottom waters based on nitrification was 1.28 and 1.49 μmol N_2O produced per mol ammonia oxidized (Table 1).

In the incubation experiments at site P05, the DIN concentrations remained unchanged (Fig. 4d) and the ammonia concentrations consistently decreased and the nitrite and nitrate concentrations increased (Fig. 4e). The rates of ammonia and nitrite oxidation were also estimated by linear regressions of ammonia and nitrate concentrations, respectively (Fig. 4d and e; Table 1). The ammonia oxidation rates were approximately equal to the sum of the increased nitrite and nitrate concentration rates. Thus, nitrification occurred during the incubation experiments without denitrification. The estimated N_2O production rates from nitrification were 1.15 nmol $L^{-1}h^{-1}$ in the P05 surface water and 1.41 nmol $L^{-1}h^{-1}$ in the P05 bottom water (Fig. 4f); the estimated N_2O yields based on nitrification were 1.03 μmol N_2O

Biogeosciences Discuss., https://doi.org/10.5194/bg-2019-132
Manuscript under review for journal Biogeosciences
Discussion started: 23 April 2019

produced per mol ammonia oxidized (surface) and 1.58 μmol N_2O produced per mol ammonia oxidized (bottom) (Table 1).

4 Discussion

4.1 Contribution of nitrification versus denitrification to N_2O production in the hypoxic upper estuary

The spatial variations of N_2O concentration, its saturation, and water-air N_2O flux along the PRE are consistent with our previous study (Lin et al., 2016), indicating that higher N_2O in the upper estuary makes the PRE acting as a source of atmospheric N_2O. The in situ incubation experiments clearly indicated that nitrification predominantly occurred in the hypoxic waters of the upper estuary along with significant N_2O production, and suggested that denitrification could be concurrent at the lowest DO site (P01) where the maximum N_2O and ΔN_2O concentrations were observed. These results confirm previous speculation that extreme enrichment of ammonia in the water column due to high loads of anthropogenic-sourced nutrients and organic matter in the upper estuary (Dai et al., 2008; He et al., 2014) could result in strong nitrification under low O_2 solubility conditions (Dai et al., 2008); thus, N_2O is produced as a byproduct through nitrification and is oversaturated in the PRE (Lin et al., 2016). The PRE sediments also act as a source of N_2O, which is released into the overlying waters through denitrification (Tan et al., 2019); however, in estuarine waters, nitrification apparently is the main source of N_2O production.

The isotopic composition of N_2O ($\delta^{15}N_{N2O}$) was consistent with the above interpretation. According to previous studies (Table S2), the $\delta^{15}N$ of N_2O produced during ammonia oxidation by AOB strains ranged from -68 to -6.7‰ (Yoshida, 1988; Sutka et al., 2006; Mandernack et al., 2009; Frame and Casciotti, 2010; Jung et al., 2014; Toyoda et al., 2017) and 6.3−10.2‰ in a marine AOA strain (Santoro et al., 2011). The $\delta^{15}N$ of N_2O produced during denitrification ranged from -37.2 to -7.9‰ (Toyoda et al., 2005); during nitrifier-denitrification by AOB strains it ranged from -57.6±4.1 to -21.5‰ (Sutka et al., 2003; Sutka et al., 2006; Frame and Casciotti, 2010). Therefore, the much lower ^{15}N-N_2O (-27.9 to -12.6‰) upstream of the Humen outlet is consistent with AOB nitrification or denitrification

processes, whereas enriched $^{15}N_2O$ (5.2−7.1‰) in the lower reaches approaches AOA nitrification and air ^{15}N-N_2O (Santoro et al., 2011). Taken together, the isotopic compositions of N_2O (Fig. 2h) and N_2O concentration distribution (Fig. 2e−g) suggest that the high concentrations of N_2O (oversaturation) were produced from strong nitrification by AOB and probably concurrent minor denitrification in the upper estuary, however in the lower reaches, low concentrations of N_2O could be explained by AOA nitrification or water atmospheric exchange of N_2O.

4.2 Correlations of nitrifiers and denitrifiers with N_2O-related biogeochemical parameters along the PRE

The more abundant AOA *amo*A genes than AOB as well as the more abundant genes in the PA communities than the FL communities are consistent with our previous study in the PRE (Hou et al., 2018), which in addition, reported significant positive correlations between the AOB *amo*A gene abundance and the oxidation rate of ammonia to nitrate. This evidence supports that AOB might be more active than AOA in the ammonium-enriched PRE (Füssel, 2014; Hou et al., 2018) despite their low abundance.

To confirm the relationship between AOA, AOB, or denitrifier and N_2O production, we analyzed the correlations between their genes abundances and N_2O-related biogeochemical parameters. The results indicate that AOA *amo*A abundance was significantly correlated (P <0.05−0.01) to the water mass parameters temperature (negatively), salinity (positively), and silicate concentration (negatively) (Table 2), suggesting that the water mass may exert control on AOA distribution. However, AOB *amo*A abundance was significantly correlated (P <0.05−0.01) to TSM concentration (positively), pH (negatively), and DO (negatively), which is consistent with our previous PRE study that found high TSM concentrations and low DO and pH influenced substrate availability and thus AOB distribution (Hou et al., 2018). Notably, there were positive correlations between AOB *amo*A abundances and all N_2O parameters as well as ammonia concentration (Table 2; P <0.05−0.01), suggesting a significant influence of AOB on N_2O production. There no significant Spearman correlations were found between bacterial nitrite reductase *nir*S abundance and the measured biogeochemical parameters.

The RDA was used to further analyze variations in the ammonia oxidizer communities under the environmental constraints. In the present study, the environmental constraints included four types: water

mass parameters (temperature, salinity, and silicate), substrate parameters (ammonia/ammonium, nitrite, and nitrate), parameters influencing substrate availability (DO, TSM, and pH), and N_2O parameters. The results confirmed that the communities with relatively high AOB abundances in the upper estuary were constrained by high temperature and low salinity water masses, high nutrient and TSM concentrations and low DO and pH conditions, as well as high N_2O concentration; whereas the opposite water masses and environmental conditions constrained the communities with high AOA abundances in the Lingdingyang area (Fig. 5). These constraints explained 87.3% of the variation in the ammonia oxidizer distribution along the PRE. Apparently, the communities with relatively high AOB abundances in the upper estuary positively influenced the concentration of N_2O in the water.

Partial Mantel tests were applied to eliminate the co-varying effects of water mass, substrate availability, and N_2O parameters along the salinity transect, and to identify the intrinsic/direct relationship between ammonia oxidizers and N_2O production. Water mass parameters (standard and partial Mantel tests, P <0.01) and those influencing substrate availability (standard and partial Mantel tests, P <0.05) significantly controlled variations in the distribution of AOA and AOB along the PRE transect (Fig. 6a and c). Notably, variations in the distribution of AOA and AOB were significantly correlated with N_2O production (standard and partial Mantel test, P <0.01) after eliminating the co-varying effects of other parameters (Fig. 6d), demonstrating the significant contribution of ammonia oxidizers to N_2O production.

4.3 Contribution of AOB versus AOA to N_2O production

We attempted to accurately assess the relative contributions of AOA and AOB to N_2O production in the PRE by plotting the N_2O production rates (Fig. 7a) and yields (Fig. 7b) normalized to total (sum of AOA and AOB) *amo*A gene copies or transcripts along X-Y axes that represent the relative contributions of AOA and AOB to the total *amo*A gene or transcript pools. The highest average *amo*A gene copy-specific N_2O production rates and yields were in the surface water of site P05, where the highest nitrification rate was also observed (Table 1). The highest average *amo*A gene transcript-specific N_2O production rates and yields were in the bottom water of site P01, where the highest N_2O production rates were observed (Table 1). Notably, for both incubation sites, the more abundant AOB

were in the *amo*A gene-based DNA or cDNA pool, the distinctly higher (disproportionately higher relative to enhanced abundance) the average *amo*A gene copy or transcript-specific N_2O production rates (Fig. 7a) and yields (Fig. 7b). Previous studies based on pure cultures of the AOB strain *Nitrosospira multiforimis* and AOA strains *Nitrososphaera viennensis* and *Nitrosopumilus maritimus* have provided evidence that AOB has higher N_2O yields (0.9 to 2.7‰) than AOA (0.3 to 0.9‰) during ammonia oxidation (Stieglmeier et al., 2014). The higher N_2O yield from AOB has also been observed in soils (Hink et al., 2017; Hink et al., 2018). Based on results indicated by Fig. 7, we conclude that AOB may have higher relative contributions to the high N_2O production in the upper estuary where low DO, high concentrations of N_2O and ΔN_2O, and high N_2O flux were observed.

Ammonia oxidizers are sensitive to oxygen during N_2O production (Santoro et al., 2011; Löscher et al., 2012; Stieglmeier et al., 2014). Studies based on pure cultures of AOB strains *Nitrosomonas marina* NM22 and *Nitrosococcus oceani* NC10 and AOA strain *Nitrosopumilus maritimus* showed higher N_2O yields and production during nitrification by both AOA and AOB when O_2 concentrations varied from aerobic to hypoxic conditions (Löscher et al., 2012). However, when O_2 concentrations varied from hypoxic to anaerobic conditions (i.e. in a lower O_2 concentration range), the AOB strain *Nitrosospira multiformis* and AOA strains *Nitrososphaera viennensis* and *Nitrosopumilus maritimus* showed that AOB had distinctly higher N_2O yields at lower oxygen conditions and, in contrast, AOA had lower N_2O yields at lower oxygen concentrations (Stieglmeier et al., 2014). In addition, results from the cultured AOB strain *Nitrosomonas marina* C-113a indicated increasing N_2O yields with higher cell concentrations (Frame and Casciotti, 2010). This evidence supports our conclusions that the high concentration of N_2O (oversaturated) may be mainly produced from strong nitrification by the high abundance of AOB in the low DO conditions in the upper estuary.

5 Conclusions

Our work explored the relative contributions of AOB and AOA in producing N_2O in the PRE by combining the isotopic compositions and concentrations of N_2O, distributions and transcript levels of AOB and AOA *amo*A and denitrifier *nir*S genes, and incubation estimates of nitrification rates and N_2O production rates. Our findings indicate that the high concentrations of N_2O and ΔN_2O and the much

Biogeosciences Discuss., https://doi.org/10.5194/bg-2019-132
Manuscript under review for journal Biogeosciences
Discussion started: 23 April 2019

lower ^{15}N-N_2O are primarily attributed to strong nitrification by AOB and probably concurrent minor denitrification in the upper estuary where AOB abundances were higher and decreased seaward along the salinity transect. Low concentrations of N_2O and ΔN_2O and enriched $^{15}N_2O$ could be explained by AOA nitrification in the lower reaches of the estuary. Collectively, AOB contributed the major part in N_2O production in the upper estuary, which is the major source of N_2O emitted to the atmosphere in the PRE.

Data availability

All data can be accessed in the form of Excel spreadsheets via the corresponding author.

The Supplement related to this article is available online.

Author contribution

M.D. and Y.Z. conceived and designed the experiments. L.M., H.L., and X.X. performed the experiments. L.M., Y.Z., H.L., and X.X. analyzed the data. L.M. and Y.Z. wrote the paper. All authors contributed to the interpretation of results and critical revision.

Competing interests

The authors declare no conflicts of interest.

Acknowledgments

We thank Qing Li for measuring ammonia concentrations on board, Jian-Zhong Su and Liguo Guo for measuring dissolved oxygen concentrations on board, and Tao Huang and Lifang Wang for measuring nitrate and nitrite concentrations. We also thank Lei Hou for her assistance in qPCR measurements and data analysis, and Mingming Chen and Huade Zhao for their assistance with the software. This research was supported by the National Key Research and Development Programs (2016YFA0601400) and NSFC projects (41676125, 41721005, and 41706086). We thank Kara Bogus, PhD, from Liwen Bianji, Edanz Editing China (www.liwenbianji.cn/ac), for editing the English text of a draft of this manuscript.

References

Allen, D., Dalal, R. C., Rennenberg, H., and Schmidt, S.: Seasonal variation in nitrous oxide and methane emissions from subtropical estuary and coastal mangrove sediments, Australia, Plant Biol., 13, 126-133, 2011.

Arévalo-Martínez, D. L., Kock, A., Löscher, C. R., Schmitz, R. A., and Bange, H. W.: Massive nitrous oxide emissions from the tropical South Pacific Ocean, Nat. Geosci., 8, 530–533, 2015.

Avrahami, S., and Bohanann, J. M.: N_2O emission rates in a California meadow soil are influenced by fertilizer level, soil moisture and the community structure of ammonia-oxidizing bacteria, Glob. Change Biol., 15, 643–655, 2009.

Bernhard, A. E., Landry, Z. C., Blevins, A., de la Torre, J. R., Giblin, A. E., and Stahl, D. A.: Abundance of ammonia-oxidizing archaea and bacteria along an estuarine salinity gradient in relation to potential nitrification rates, Appl. Environ. Microbiol., 76, 1285–1289, 2010.

Braker, G., Fesefeldt, A., and Witzel, K. P.: Development of PCR primer systems for amplification of nitrite reductase genes (*nir*K and *nir*S) to detect denitrifying bacteria in environmental samples, Appl. Environ. Microbiol., 64, 3769–3775, 1998.

Butterbach-Bahl, K., Baggs, E. M., Dannenmann, M., Kiese, R., and Zechmeister-Boltenstern, S.: Nitrous oxide emissions from soils: how well do we understand the processes and their controls? Philos. Trans. R. Soc. B-Biol. Sci., 368, https://doi.org/10.1098/rstb.2013.0122, 2013.

Canfield, D. E., Glazer, A. N., and Falkowski, P. G.: The Evolution and Future of Earth's Nitrogen Cycle, Science, 330, 192–196, 2010.

Cao, Y., Sun, G., Han, Y., Sun, D., and Wang, X.: Determination of nitrogen, carbon and oxygen stable isotope ratios in N_2O, CH_4, and CO_2 at natural abundance levels by mass spectrometer, Acta. Pedologica. Sinica., 45, 249–258, 2008 (Chinese).

Clark, I. M., Buchkina, N., Jhureea, D., Goulding, K. W. T., and Hirsch, P. R.: Impacts of nitrogen application rates on the activity and diversity of denitrifying bacteria in the Broadbalk Wheat Experiment, Philos. Trans. R. Soc. B-Biol. Sci., 367, https://doi.org/10.1098/rstb.2011.0314, 2012.

Čuhel, J., Šimek, M., Laughlin, R. J., Bru, D., Chèneby, D., Watson, C. J., and Philippot, L.: Insights into the Effect of Soil pH on N_2O and N_2 Emissions and Denitrifier Community Size and Activity, Appl. Environ. Microbiol., 76, 6, 1870–1878, 2010.

Dai, M., Guo, X., Zhai, W., Yuan, L., Wang, B., Wang, L., Cai, P., Tang, T., and Cai, W. J.: Oxygen depletion in the upper reach of the Pearl River estuary during a winter drought, Mar. Chem., 102, 159–169, 2006.

Dai, M., Wang, L., Guo, X., Zhai, W., Li, Q., He, B., and Kao, S. J.: Nitrification and inorganic nitrogen distribution in a large perturbed river/estuarine system: the Pearl River Estuary, China, Biogeosciences, 5, 1545–1585, 2008.

Dai, M., Gan, J., Han, A., Kung, H. S., and Yin, Z.: Physical dynamics and biogeochemistry of the Pearl River plume, In Biogeochemical dynamics at major river-coastal interfaces, Linkages with Global Change. Bianchi, T. S., Allison, M. A., and Cai, W. J. (eds). Cambridge University Press, pp. 321–351, 2014.

Frame, C. H., and Casciotti, K. L.: Biogeochemical controls and isotopic signatures of nitrous oxide production by a marine ammonia-oxidizing bacterium, Biogeosciences, 7, 2695–2709, 2010.

Frame, C. H., Lau, E., Joseph Nolan IV, E., Goepfert, T. J., and Lehmann, M. F.: Acidification Enhances Hybrid N_2O Production Associated with Aquatic Ammonia-Oxidizing Microorganisms, Front. Microbiol., 7, 1–23, 2017.

Francis, C. A., Roberts, K. J., Beman, J. M., Santoro, A. E., and Oakley, B. B.: Ubiquity and diversity of ammonia-oxidizing archaea in water columns and sediments of the ocean, P. Natl. Acad. Sci. USA, 102, 14683–14688, 2005.

Freing, A., Wallace, D. W. R., and Bange, H. W.: Global oceanic production of nitrous oxide, Philos. Trans. R. Soc. B-Biol. Sci., 367, https://doi.org/10.1098/rstb. 2011. 0360, 2012.

Füssel, J.: Impacts and importance of ammonia and nitrite oxidation in the marine nitrogen cycle, PhD thesis, Max Planck Institute for Microbial Ecology, Bremen, Germany, 166 pp., 2014.

Han, A., Dai, M., Kao, S.-J., Gan, J., Li, Q., Wang, L., Zhai, W., and Wang, L.: Nutrient dynamics and biological consumption in a large continental shelf system under the influence of both a river plume and coastal upwelling, Limnol. Oceanogr., 57, 486–502, 2012.

Hatzenpichler, R.: Diversity, Physiology, and Niche Differentiation of Ammonia Oxidizing Archaea, Appl. Environ. Microbol., 78, 7501–7510, 2012.

He, B., Dai, M., Zhai, W., Guo, X., and Wang, L.: Hypoxia in the upper reaches of the Pearl River Estuary and its maintenance mechanisms: A synthesis based on multiple year observations during 2000-2008, Mar. Chem., 167, 13–24, 2014.

Hink, L., Nicol, G. W., and Prosser, J. I.: Archaea produce lower yields of N_2O than bacteria during aerobic ammonia oxidation in soil, Environ. Microbiol., 19, 4829–4837, 2017.

Hink, L., Gubry-Rangin, C., Nicol, G. W., and Prosser, J. I.: The consequences of niche and physiological differentiation of archaeal and bacterial ammonia oxidisers for nitrous oxide emissions, ISME J., 12,1084–1093, 2018.

Hou, L., Xie, X., Wan, X., Kao, S. J., Jiao, N., and Zhang, Y.: Niche differentiation of ammonia and nitrite oxidizers along a salinity gradientnfrom the Pearl River estuary to the South China Sea, Biogeosciences, 15, 5169–5187, 2018.

Huang, S., Chen, C., Yang, X., Wu, Q., and Zhang, R.: Distribution of typical denitrifying functional genes and diversity of the *nir*S-encoding bacterial community related to environmental characteristics of river sediments, Biogeosciences, 8, 3041–3051, 2011.

Hu, A., Jiao, N., and Zhang, C. L.: Community structure and function of planktonic *Crenarchaeota*: changes with depth in the South China Sea, Microb. Ecol., 62, 549–563, 2011.

Jones, C. M., Spor, A., Brennan, F. P., Breuil, M. C., Bru, D., Lemanceau, P., Griffiths, B., Hallin, S., and Philippot, L.: Recently identified microbial guild mediates soil N_2O sink capacity, Nat. Clim. Chang., 4, 801–805, 2014.

Jung, M. Y., Well, R., Min, D., Giesemann, A., Park, S. J., Kim, J. G., and Rhee, S. K.: Isotopic signatures of N_2O produced by ammonia-oxidizing archaea from soils, ISME J., 8, 1115–1125, 2014.

Kim, O. S., Junier, P., Imhoff, J. F., and Witzel, K. P.: Comparative analysis of ammonia monooxygenase (*amo*A) genes in the water column and sediment–water interface of two lakes and the Baltic Sea, FEMS Microbiol. Ecol., 66, 367–378, 2008.

Kroeze, C., Dumont, E., and Seitzinger, S.: Future trends in emissions of N_2O from rivers and estuaries, J. Integr. Environ. Sci., 7, 71–78, 2010.

Lin, H., Dai, M., Kao, S. J., Wang, L., Roberts, E., Yang, J., Huang, T., and He, B.: Spatiotemporal variability of nitrous oxide in a large eutrophic estuarine system: The Pearl River Estuary, China, Mar. Chem., 182, 14–24, 2016.

Löscher, C. R., Kock, A., Könneke, M., LaRoche, J., Bange, H. W., and Schmitz, R. A.: Production of oceanic nitrous oxide by ammonia-oxidizing archaea, Biogeosciences, 9, 2419–2429, 2012.

Magalhães, C., Bano, N., Wiebe, W. J., Bordalo, A. A., and Hollibaugh, J. T.: Dynamics of nitrous oxide reductase genes (*nosZ*) in intertidal rocky biofilms and sediments of the Douro River Estuary (Portugal), and their relation to N-biogeochemistry, Microb. Ecol., 55, 259–269, 2008.

Mandernack, K. W., Mills, C. T., Johnson, C. A., Rahn, T., and Kinney, C.: The $\delta^{15}N$ and $\delta^{18}O$ values of N_2O produced during the co-oxidation of ammonia by methanotrophic bacteria, Chem. Geol., 267, 96–107, 2009.

Mincer, T. J., Church, M. J., Taylor, L. T., Preston, C., Karl, D. M., and DeLong, E. F.: Quantitative distribution of presumptive archaeal and bacterial nitrifiers in Monterey Bay and the North Pacific Subtropical Gyre, Environ. Microbiol., 9, 1162–1175, 2007.

Monteiro, M., Séneca, J., and Magalhães, C.: The History of Aerobic Ammonia Oxidizers: from the First Discoveries to Today, J. Microbiol., 52, 537–547, 2014.

Mortazavi, B., Iverson, R. L., Huang, W., Graham Lewis, F., Caffrey, J. M.: Nitrogen budget of Apalachicola Bay, a bar-built estuary in the northeastern Gulf of Mexico, Mar. Ecol.-Prog. Ser., 195, 1–14, 2000.

Naqvi, S. W. A., Bange, H. W., Farías, L., Monteiro, P. M. S., Scranton, M. I., and Zhang, J.: Marine hypoxia/anoxia as a source of CH_4 and N_2O, Biogeosciences, 7, 2159–2190, 2010.

Nevison, C. D., Lueker, T. J., and Weiss, R. F.: Quantifying the nitrous oxide source from coastal upwelling, Glob. Biogeochem. Cycle, 18, 1–17, 2004.

Ni, B. J., Peng, L., Law, Y., Guo, J., and Yuan, Z.: Modeling of Nitrous Oxide Production by Autotrophic Ammonia-Oxidizing Bacteria with Multiple Production Pathways, Environ. Sci. Technol., 48, 3916–3924, 2014.

Pai, S. C., Tsau, Y. J., and Yang, T. I.: pH and buffering capacity problems involved in the determination of ammonia in saline water using the indophenol blue spectrophotometric method, Analytica Chimica Acta, 434, 209–216, 2001.

Rabalais, N. N., D´ıaz, R. J., Levin, L. A., Turner, R. E., Gilbert, D., and Zhang, J.: Dynamics and distribution of natural and human-caused hypoxia, Biogeosciences, 7, 585–619, 2010.

Ravishankara, A. R., Daniel, J. S., and Portmann, R. W.: Nitrous Oxide (N_2O): The Dominant Ozone-Depleting Substance Emitted in the 21st Century, Science, 326, 123–125, 2009.

Raymond, P. A., and Cole, J. J.: Gas exchange in rivers and estuary: choosing a gas transfer velocity, Estuaries Coasts, 24, 312–317, 2001.

Santoro, A. E., Buchwald, C., McIlvin, M. R., and Casciotti K. L.: Isotopic Signature of N_2O Produced by Marine Ammonia-Oxidizing Archaea, Science, 333, 1282–1285, 2011.

Seitzinger, S. P., and Kroeze, C.: Global distribution of nitrous oxide production and N inputs in freshwater and coastal marine ecosystems, Glob. Biogeochem. Cycle, 12, 93-113, 1998.

Shaw, L. J., Nicol, G. W., Smith, Z., Fear, J., Prosser, J. I., Baggs, E. M.: *Nitrosospira* spp. can produce nitrous oxide via a nitrifier denitrification pathway, Environ. Microbiol., 8, 214–222, 2006.

Stein, L. Y.: Surveying N_2O-Producing Pathways in Bacteria, Methods Enzymol., 486, 131–152, 2011.

Stieglmeier, M., Mooshammer, M., Kitzler, B., Wanek, W., Zechmeister-Boltenstern, S., Richter, A., and Schleper, C.: Aerobic nitrous oxide production through N-nitrosating hybrid formation in ammonia-oxidizing archaea, ISME J., 8, 1135–1146, 2014.

Sutka, R. L., Ostrom, N. E., Ostrom, P. H., Gandhi, H., and Breznak, J. A.: Nitrogen isotopomer site preference of N_2O produced by Nitrosomonas europaea and Methylococcus capsulatus Bath, Rapid Commun. Mass Spectrom., 17, 738–745, 2003.

Sutka, R. L., Ostrom, N. E., Ostrom, P. H., Breznak, J. A., Gandhi, H., Pitt, A. J., and Li, F.: Distinguishing Nitrous Oxide Production from Nitrification and Denitrification on the Basis of Isotopomer Abundances, Appl. Environ. Microbiol., 72, 638–644, 2006.

Syakila, A., and Kroeze, C.: The global nitrogen budget revisited, J. Greenhouse Gas Meas. Manag., 1, 17–26, 2011.

Tan, E., Zou, W., Jiang, X., Wan, X., Hsu, T. C., Zheng, Z., Chen, L., Xu, M., Dai, M., Kao, S.: Organic matter decomposition sustains sedimentary nitrogen loss in the Pearl River Estuary, China, Sci. Total. Environ., 648, 508–517, 2019

Toyoda, S., Mutobe, H., Yamagishi, H., Yoshida, N., Tanji, Y.: Fractionation of N_2O isotopomers during production by denitrifier, Soil. Biol. Biochem., 37, 1535–1545, 2005.

Toyoda, S., Yoshida, N., and Koba, K.: Isotopocule analysis of biologically produced nitrous oxide in various environments, Mass Spectrom. Rev., 36, 135–160, 2017.

Usui, T., Koike, I., and Ogura, N.: N_2O production, nitrification and denitrification in an estuarine sediment, Estuar. Coast. Shelf Sci., 52, 769-781, 2001.

Voss, M., Bange, H. W., Dippner, J. W., Middelburg, J. J., Montoya, J. P., and Ward, B.: The marine nitrogen cycle: recent discoveries, uncertainties and the potential relevance of climate change, Philos. Trans. R. Soc. B-Biol. Sci., 368, 20130121, 2013.

Wanninkhof, R. I. K.: Relationship between wind speed and gas exchange over the ocean, J. Geophys. Res.-Oceans, 97, 7373–7382, 1992.

Weiss, R. F., and Price, B. A.: Nitrous oxide solubility in water and seawater, Mar. Chem., 8, 347–359, 1980.

Yoshida, N.: ^{15}N-depleted N_2O as a product of nitrification, Nature, 335, 528–529, 1988.

Yu, R., Kampschreur, M. J., Mark van Loosdrecht, C. M., and Chandran, K.: Mechanisms and Specific Directionality of Autotrophic Nitrous Oxide and Nitric Oxide Generation during Transient Anoxia, Environ. Sci. Technol., 44, 1313–1319, 2010.

Zhang, Y., Xie, X., Jiao, N., Hsiao, S. S. Y., and Kao, S. J.: Diversity and distribution of *amoA*-type nitrifying and *nir*S-type denitrifying microbial communities in the Yangtze River estuary, Biogeosciences, 11, 2131–2145, 2014.

Zhu, R., Liu, Y., Li, X., Sun, J., Xu, H. and Sun, L.: Stable isotope natural abundance of nitrous oxide emitted from Antarctic tundra soils: effects of sea animal excrement depositions, Rapid Commun. Mass Spectrom., 22, 3570–3578, 2008.

Biogeosciences Discuss., https://doi.org/10.5194/bg-2019-132
Manuscript under review for journal Biogeosciences
Discussion started: 23 April 2019

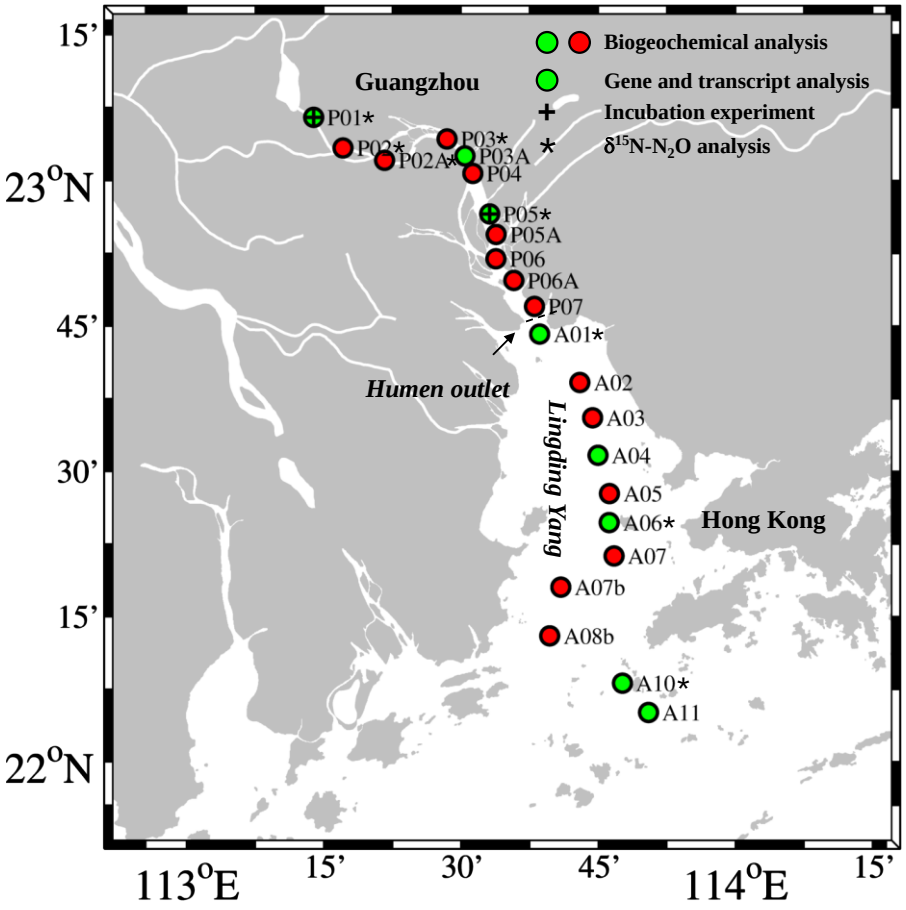

Figure 1: Map of the Pearl River Estuary showing the sampling sites. Biogeochemical analyses were performed on samples from all sites. The green circles indicate sites from which genes and transcripts were analyzed. The black crosses indicate in situ incubation experiment sites. The black asterisks indicate samples from which the isotopic composition of N_2O was analyzed.

Biogeosciences Discuss., https://doi.org/10.5194/bg-2019-132
Manuscript under review for journal Biogeosciences
Discussion started: 23 April 2019

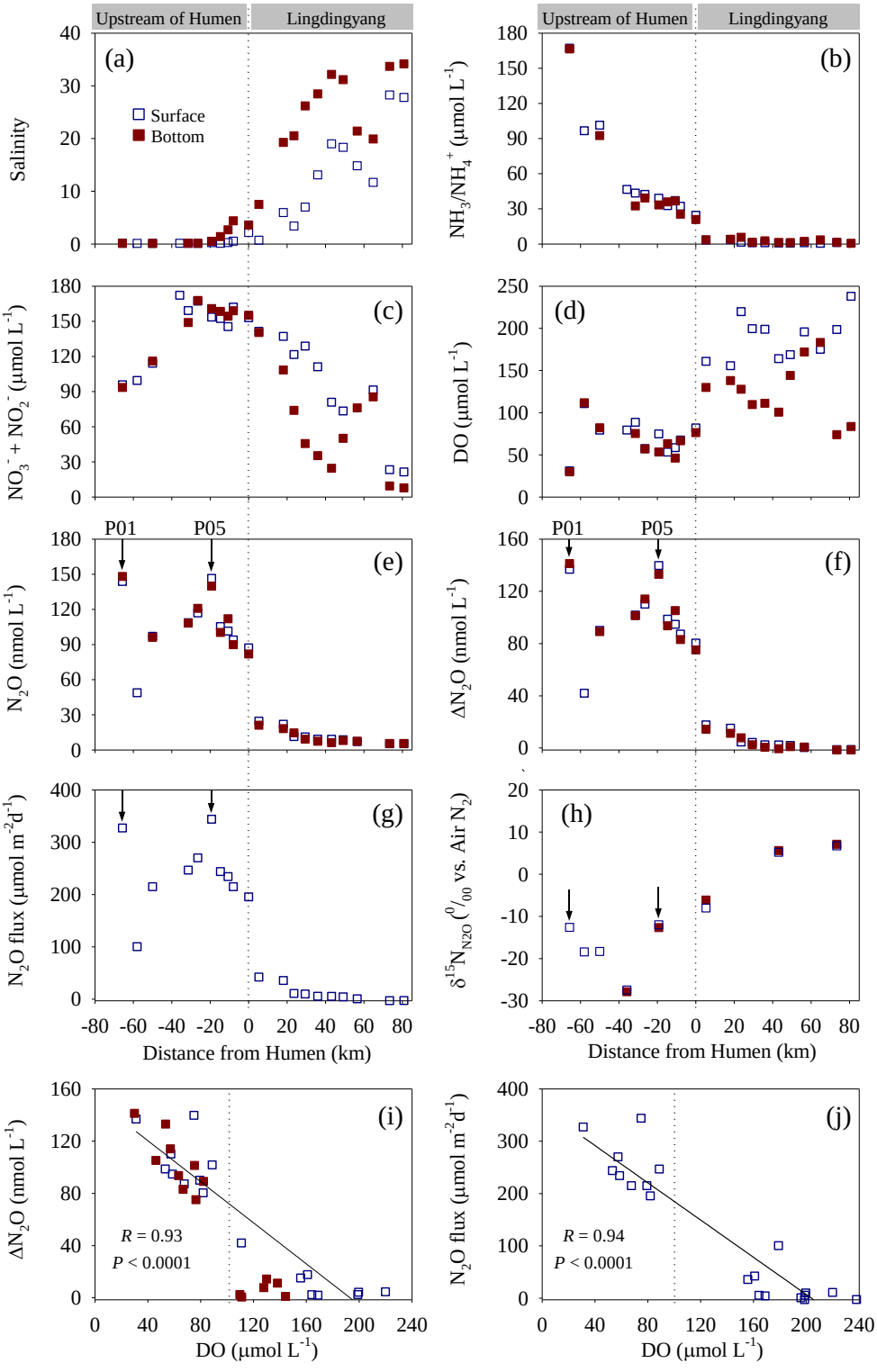

Biogeosciences Discuss., https://doi.org/10.5194/bg-2019-132
Manuscript under review for journal Biogeosciences
Discussion started: 23 April 2019

Figure 2: Distribution of biogeochemical factors along the PRE transect. (a) Salinity, (b) NH_3/NH_4^+, (c) $NO_2^- + NO_3^-$, (d) DO, (e) N_2O, and (f) ΔN_2O concentration, (g) N_2O flux, (h) $\delta^{15}N_{N2O}$, (i) ΔN_2O vs. DO, and (j) N_2O flux vs. DO. The dashed lines show the division of the transect into the northern (upstream of the Humen outlet) and southern (Lingdingyang) areas. The arrows indicate the sites where the in situ incubation experiments were performed.

Biogeosciences Discuss., https://doi.org/10.5194/bg-2019-132
Manuscript under review for journal Biogeosciences
Discussion started: 23 April 2019

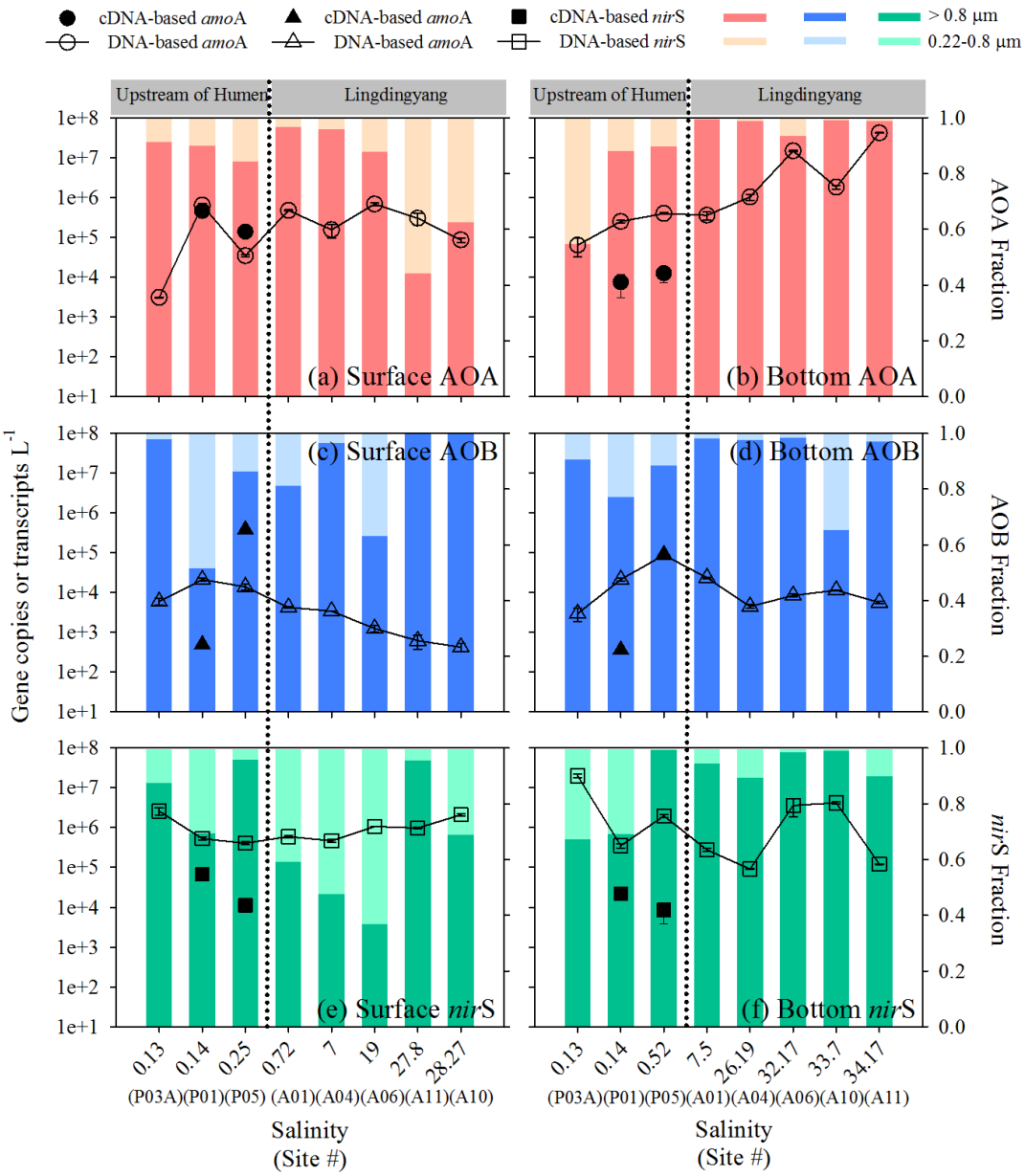

Figure 3: Abundance distribution of AOA and AOB *amo*A and bacterial *nir*S along the salinity gradient in the PRE. Abundances of AOA *amo*A genes (open circles) and PA transcripts (closed circles) and the relative abundances of PA and FL AOA *amo*A genes in (a) surface water and (b) bottom water. Abundances of AOB *amo*A genes (open triangles) and PA transcripts (closed triangles) and the relative abundances of PA and FL AOB *amo*A genes in (c) surface water and (d) bottom water. Abundance of bacterial *nir*S genes (open squares) and PA transcripts (closed squares) and the relative abundances of

Biogeosciences Discuss., https://doi.org/10.5194/bg-2019-132
Manuscript under review for journal Biogeosciences
Discussion started: 23 April 2019

PA and FL *nir*S genes in (e) surface water and (f) bottom water. The dashed lines indicate the division into the northern (upstream of the Humen outlet) and southern (Lingdingyang) areas.

Biogeosciences Discuss., https://doi.org/10.5194/bg-2019-132
Manuscript under review for journal Biogeosciences
Discussion started: 23 April 2019

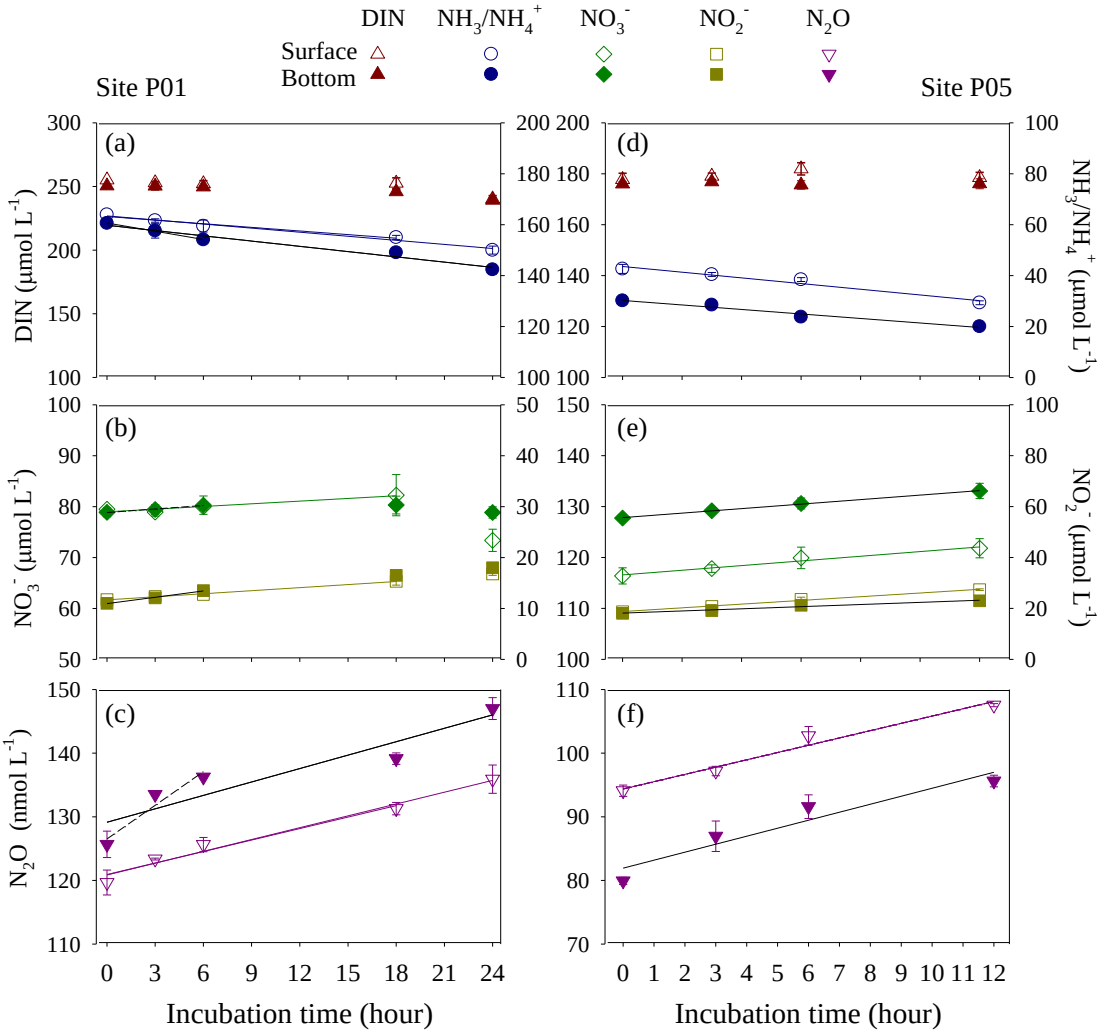

Figure 4: Variations in nitrogen compounds and N_2O concentrations at sites P01 and P05 during the incubation experiments in surface (open symbols) and bottom (closed symbols) waters. (a, d) Total DIN (brown triangles) and NH_3/NH_4^+ (blue circles); (b, e) NO_3^- (green diamonds) and NO_2^- (dark yellow squares); (c, f) N_2O (purple inverted triangles). Linear regressions depend on whether variations in DIN concentration against time retain "mass balance" in a closed incubation system. The linear regressions of ammonia were used to estimate ammonia oxidation rates in (a) P01 over 18 and 24 h (surface, blue lines) and 6 and 24 h (bottom, black lines), and (d) P05 over 12 h (surface, blue line; bottom, black line). The linear regressions of nitrate estimated nitrite oxidation rates in (b) P01 over 18 h (surface water, green line) and 6 h (bottom water, black line), and (e) P05 after 12 h (surface, green line; bottom, black

Biogeosciences Discuss., https://doi.org/10.5194/bg-2019-132
Manuscript under review for journal Biogeosciences
Discussion started: 23 April 2019

line). The nitrite linear regressions after 18 h (surface water, dark yellow line) and 6 h (bottom water, black line) in P01 and 12 h (surface, dark yellow line; bottom, black line) in P05 are also shown, but do not indicate oxidation rates. The N_2O linear regressions were used to estimate N_2O production rates in (c) P01 after 18 and 24 h (surface water, purple lines) and 6 and 24 h (bottom water, black lines; dashed line, no statistical significance test), and (f) P05 after 12 h (surface, purple line; bottom, black line). All regression formulas, R, and *P* values are shown in Table 1.

Biogeosciences Discuss., https://doi.org/10.5194/bg-2019-132
Manuscript under review for journal Biogeosciences
Discussion started: 23 April 2019

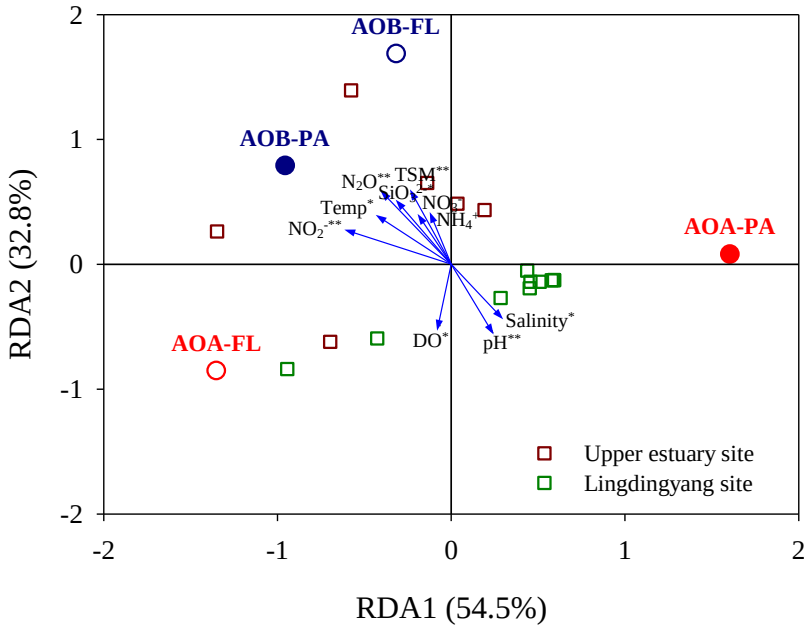

Figure 5: Redundancy analysis of ammonia-oxidizing communities under biogeochemical constraints. Each square represents an individual community. Vectors represent environmental variables. Temp, temperature. $^{*}P$ <0.05, $^{**}P$ <0.01 (Monte Carlo permutation test).

Biogeosciences Discuss., https://doi.org/10.5194/bg-2019-132
Manuscript under review for journal Biogeosciences
Discussion started: 23 April 2019

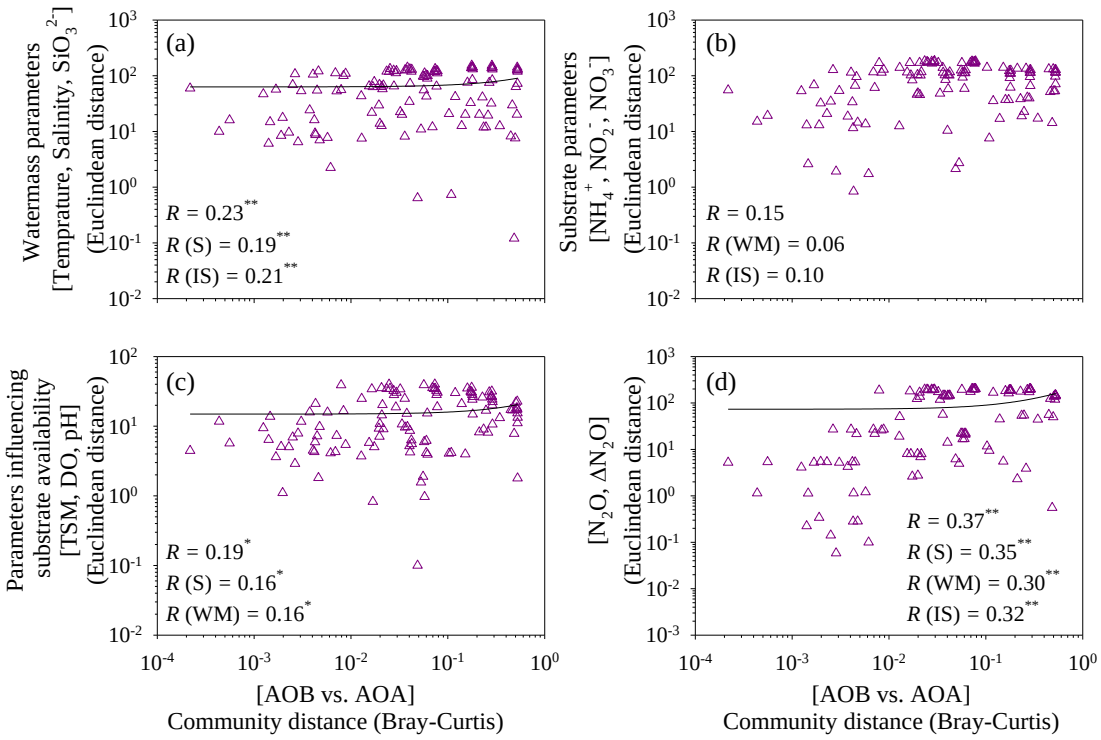

Figure 6: Correlations between ammonia oxidizer community composition and (a) water mass parameters (temperature, salinity, and silicate), (b) substrate parameters (ammonia/ammonium, nitrite, and nitrate), (c) parameters influencing substrate availability (TSM, DO, and pH), or (d) N_2O parameters (N_2O and ΔN_2O). The ammonia oxidizer community matrix was calculated according to AOA and AOB abundances. Dissimilarity matrices of communities were based on Bray-Curtis distances and environmental factors were based on Euclidean distances between samples. Standard and partial Mantel tests were run to measure the correlation between two matrices. Spearman or Kendall's correlation coefficient (R) values are shown for standard (first value) and partial Mantel (second, third, and fourth) tests. The *P* values were calculated using the distribution of the Mantel test statistics estimated from 999 permutations. $^{*}P < 0.05$; $^{**}P < 0.01$.

Biogeosciences Discuss., https://doi.org/10.5194/bg-2019-132
Manuscript under review for journal Biogeosciences
Discussion started: 23 April 2019

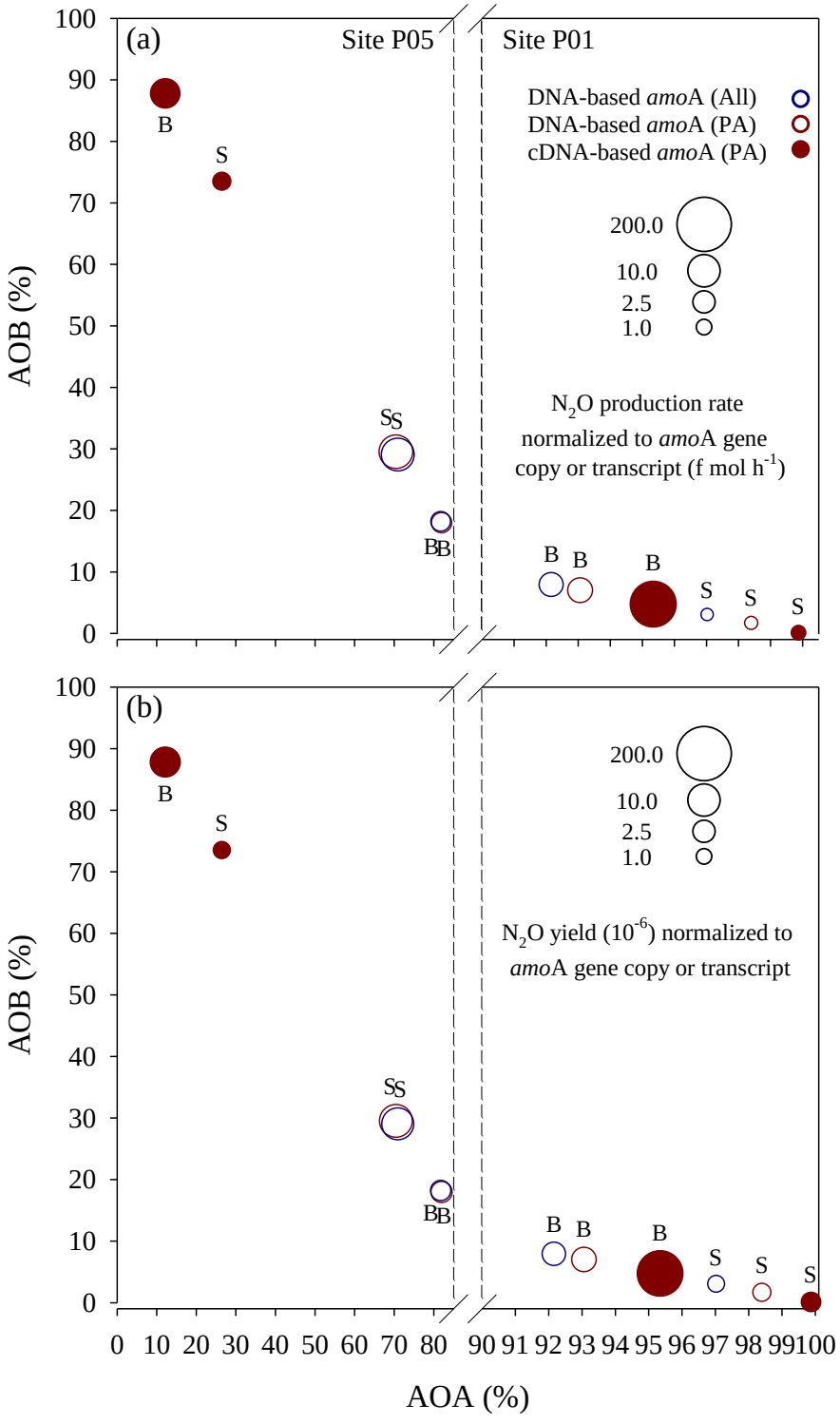

Biogeosciences Discuss., https://doi.org/10.5194/bg-2019-132
Manuscript under review for journal Biogeosciences
Discussion started: 23 April 2019

Figure 7: N_2O (a) production rates and (b) yields normalized to total *amo*A gene copy or transcript numbers of AOA and AOB in a given sample. They are presented along the x-y axes that represent the relative contributions of AOA and AOB to the total *amo*A gene or transcript pools. S, surface; B, bottom.

Biogeosciences Discuss., https://doi.org/10.5194/bg-2019-132
Manuscript under review for journal Biogeosciences
Discussion started: 23 April 2019

Table 1 Linear regressions of ammonia, nitrite, nitrate, and N_2O concentrations against time and N_2O yields during incubation experiments.

Site_Layer	Time (hour)	$\Delta NH_3/NH_4^+$ (μmol L^{-1} h^{-1})			ΔNO_2^- (μmol L^{-1} h^{-1})			ΔNO_3^- (μmol L^{-1} h^{-1})			ΔN_2O (nmol $L^{-1}h^{-1}$)			N_2O yield[a]
		Liner Regression	*R*	Rate	Liner Equation	*R*	Rate	Liner Regression	*R*	Rate	Liner Regression	*R*	Rate	
P01_S	18	$y = -0.47x+163.20$	0.98^{*}	0.47	$y = 0.20x+11.69$	1.00^{**}	0.20	$y = 0.18x+78.98$	0.95^{*}	0.18	$y = 0.60x+120.93$	0.98^{*}	0.60^{b}	1.28^{b}
	24	$y = -0.53x+163.44$	0.99^{**}	0.53	–	–	–	–	–	–	$y = 0.62x+120.85$	0.99^{**}	0.62	–[c]
P01_B	6	$y = -1.08x+160.65$	1.00^{*}	1.08	$y = 0.42x+10.95$	1.00^{*}	0.42	$y = 0.23x+78.84$	0.99	0.23	$y = 1.61x+127.04$	0.99	1.61^{b}	1.49^{b}
	24	$y = -0.69x+159.76$	0.98^{**}	0.69	–	–	–	–	–	–	$y = 0.70x+129.14$	0.93^{*}	0.70	–[c]
P05_S	12	$y = -1.12x+43.58$	0.98^{*}	1.12	$y = 0.73x+18.78$	1.00^{**}	0.73	$y = 0.46x+116.58$	0.99^{**}	0.46	$y = 1.15x+79.79$	0.99^{**}	1.15^{b}	1.03^{b}
P05_B	12	$y = -0.89x+30.25$	0.98^{*}	0.89	$y = 0.42x+18.17$	0.98^{*}	0.42	$y = 0.44x+127.83$	1.00^{**}	0.44	$y = 1.41x+81.57$	0.98^{*}	1.41^{b}	1.58^{b}

[a]μmol N_2O produced per mol ammonia oxidized.

[b]These rates and yields (when only nitrification occurred) were used to calculate the average *amo*A gene copy-specific N_2O production rates and N_2O yields in Figure 7.

[c]No estimation of N_2O yield was made due to nitrification and denitrification may occur concurrently.

$^{*}P < 0.05$; $^{**}P < 0.01$.

–No regression analysis or no estimation made.

Biogeosciences Discuss., https://doi.org/10.5194/bg-2019-132
Manuscript under review for journal Biogeosciences
Discussion started: 23 April 2019

Table 2 R values for the relationships between nitrifier and denitrifier gene abundances and biogeochemical parameters in the PRE.

Biogeochemical parameters	PA + FL			PA (> 0.8 μm)			FL (0.22–0.8 μm)		
	AOA-*amo*A (n =16)	AOB-*amo*A (n =16)	*nir*S (n =16)	AOA-*amo*A (n =16)	AOB-*amo*A (n =14)	*nir*S (n =16)	AOA-*amo*A (n =16)	AOB-*amo*A (n =16)	*nir*S (n =16)
Temperature	-0.694**	0.359	0.085	-0.676**	0.303	0.165	-0.438	0.358	0.229
Salinity	0.644**	-0.339	-0.018	0.604*	-0.270	-0.047	0.403	-0.351	-0.356
SiO_3^-	-0.541*	0.559*	0.206	-0.497	0.503*	0.282	-0.350	0.481	0.238
TSM	-0.109	0.668**	0.047	-0.097	0.612*	0.194	0.191	0.565*	-0.071
pH	0.381	-0.656**	0.157	0.316	-0.615*	0.088	0.377	-0.605*	-0.059
DO	-0.074	-0.771**	-0.026	-0.121	-0.729**	-0.144	0.009	-0.697**	0.218
NH_3/NH_4^+	-0.482	0.646**	0.068	-0.482	0.571*	0.196	-0.325	0.587*	0.000
NO_3^-	-0.485	0.359	-0.138	-0.444	0.353	-0.112	-0.588*	0.213	0.115
NO_2^-	-0.588*	0.447	0.126	-0.556*	0.356	0.212	-0.421	0.288	0.265
N_2O	-0.421	0.641**	-0.194	-0.356	0.606*	-0.121	-0.385	0.490	0.047
ΔN_2O	-0.527*	0.559*	-0.160	-0.480	0.517*	-0.081	-0.369	0.504	0.096
N_2O flux[a]	-0.190 (n = 8)	1.000** (n = 8)	-0.524 (n = 8)	-0.143 (n = 8)	1.000** (n = 8)	-0.310 (n = 8)	-0.571 (n = 8)	0.657 (n = 6)	-0.524 (n = 8)

[a]Surface data; *P <0.05; **P <0.01.